Pergamon

Int. J. Solids Structures Vol. 34, No. 6, pp. 755–768, 1997

0020–7683/97 $17.00 + .00

PII: S0020–7683(96)00045–5

LARGE DEFLECTIONS OF SHELLS SUBJECTED TO AN EXTERNAL LOAD AND TEMPERATURE CHANGES

JAKUB MARCINOWSKI
Technical University of Wrocław, Institute of Civil Engineering, Wybrzeże Wyspiańskiego 27, 50-370 Wrocław, Poland

(*Received* 21 *October* 1994; *in revised form* 6 *March* 1995)

Abstract—Shell stability in geometrically nonlinear range is considered. Influence of the temperature change on the value of the critical force is examined. The whole analysis is performed numerically using the Finite Element Method. To solve the problem, nonlinear equilibrium paths for given temperature change and various load values must be calculated. These are cross-sections of the nonlinear equilibrium surface. From such paths the critical value of the load for given temperature change can be determined and stability boundary can be found as the main purpose of the procedure. The detailed numerical analysis was performed in reference to the semi cylindrical shell segment subjected to temperature changes and loaded by the concentrated force. Copyright © 1997 Published by Elsevier Science Ltd.

1. INTRODUCTION

The large deflection analysis of flexible structures is usually confined to structures sustaining an external load only. It is obvious that the external loads are of the highest importance as far as the stability phenomenon is concerned. There are other factors that can also violate the stable equilibrium configuration and cause failure of the structure. The temperature change is an example of such a factor.

Attention will be focused on laterally loaded shallow shells which seem to be highly sensitive to temperature changes. The properly designed shell panels have to sustain external loads in various environmental conditions. For a given value of the temperature change, the critical value of the external load must be known. The main subject of interest of the present paper is the establishment of relationship between temperature change and critical value of external load.

To define precisely the scope of the paper let us look closely at such a problem. The most typical nonlinear response of the flexible structure is presented in Fig. 1. Point B stands for the bifurcation point, point T—turning point, points U and L—upper and lower limit points, respectively. Let us assume that the structure is subjected to temperature changes and then is loaded by the external load defined by the load intensity parameter λ. The question arises: what will be the load–displacement characteristic at this new temperature and particularly, what will be the value of the critical load? This is the problem which will be focused in the paper and it is worthy to emphasise that in such problems both the temperature decrease or its increase can cause the structural failure.

The nonlinear response shown in Fig. 1 is adequate to one parameter loading. Taking into account the temperature change means that two independent load factors are considered. As a result, instead of the equilibrium path shown in Fig. 1 the equilibrium surface like that shown in Fig. 2 must be determined. In this case instead of critical points the critical zone must be located and its projection on λ_1 (load)–λ_2 (temperature change) subspace must be found. This projection is called the stability boundary (see Husein, 1975) and its knowledge is the most important from practical point of view.

To locate the equilibrium surface in the load–temperature change–displacement space, the nonlinear equilibrium equations are required. Derivation of these equations in the case when the structure is subjected to external load and as well as temperature change is

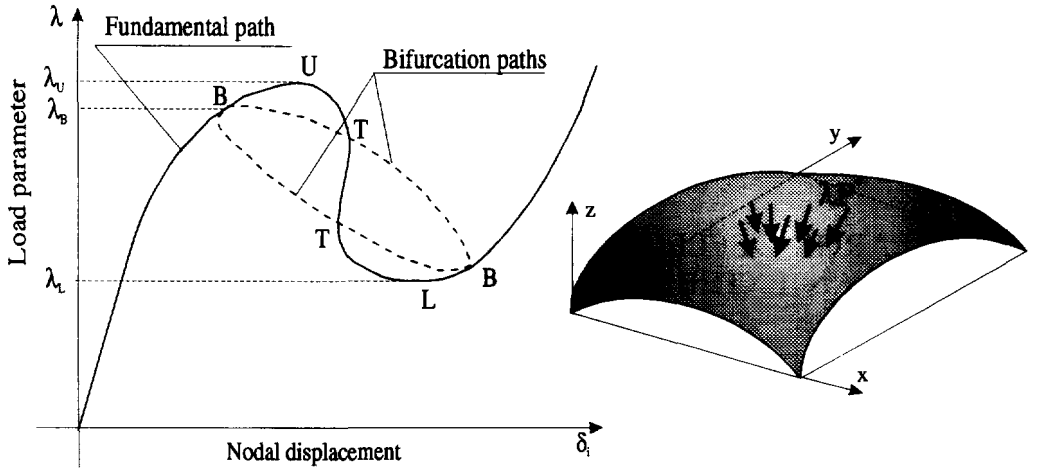

Fig. 1. Typical nonlinear response of a laterally loaded shell panel.

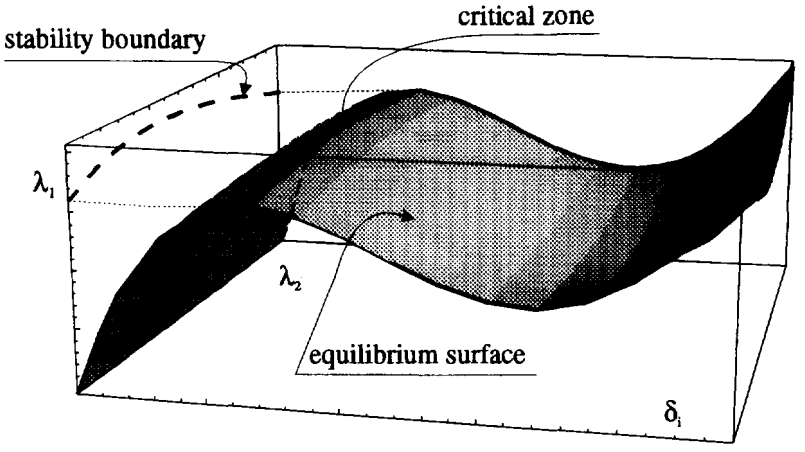

Fig. 2. Equilibrium surface in a case of two parameter loading.

presented in the paper. Equilibrium equations are derived for the discrete model and finite element method is applied to discretize the domain of the shell.

As far as the principal assumptions are concerned, it will be assumed that only linear stress–strain relations will hold but as far as displacements are concerned, no limits will be specified. All material constants are not temperature dependent and temperature distribution will be constant in the whole domain.

A review of all papers dealing with shell stability problems in which the temperature effects were taken into account appeared recently (Thornton, 1993). It follows from it that most of the papers have dealt with cylindrical shells supported at the ends. The critical temperature elevation was found by the solution of the eigenvalue problem to which the problem can be reduced. This very typical approach called the linear stability or the initial stability was also adopted by Chen and Chen (1990), where many other references from this field were listed.

The validity of such an approach is confined to these cases when the displacements remain small in the prebuckling state. It leads to significant errors if the prebuckling displacements are highly nonlinear. Laterally loaded shell panels are examples of such structures. They are very flexible and from the very beginning to the buckling configurations one observes the large displacements. For such problems the linear stability approach must be replaced by the full geometrically nonlinear analysis. It means that the critical configurations must be determined in the calculation process of the nonlinear equilibrium path with all its singular points.

There also exist studies which deal with large deformations of plates due to temperature changes. It is worthy to mention two of them. These are studies of Sivakumaran (1990)

and of Meyers and Hyer (1991). Papers of Chen and Chen (1991) and Huang and Tauchert (1991) deal with large deformations of laminated cylindrical panels. In both the numerical approach with the finite element method was adopted.

2. GOVERNING EQUATIONS. GENERAL CASE

The nonlinear equilibrium surface is the set of equilibrium configurations in the $N+2$ dimensional (N is the number of degrees of freedom of the discretized system) load–temperature change–displacement space. Every configuration (the point on this surface) is the result of the solution of the nonlinear equilibrium equations. These equations can be obtained, in the general case, as follows.

Let us start from the principle of the virtual displacements. If δd_i denotes the virtual displacements of the discretized three-dimensional system, then this principle can be expressed as follows:

$$\int_v \delta\varepsilon^k \sigma^k \, \mathrm{d}V - \lambda F_i^P \delta d_i = 0, \tag{1}$$

where $\delta\varepsilon^k$ is the variation of the k-th strain component due to the nodal displacement variation (below, the FEM in displacement formulation will be adopted), σ^k is the k-th stress component, λF_i^P denotes the generalised nodal forces which correspond to the nodal displacements, λ is the parameter of load intensity and F_i^P refers to external loads at reference level.

For isotropic, linearly elastic material the stress strain relation adopts the Duhamel-Neumann's form (see Wempner, 1981) in which temperature effects are taken into account:

$$\sigma_{ij} = 2G\varepsilon_{ij} + \Lambda\varepsilon_{kk}\delta_{ij} - \alpha(3\Lambda + 2G)\Delta T\delta_{ij}, \quad i,j,k = 1,\ldots 3, \tag{2}$$

where Λ, G are Lame's constants, δ_{ij} is the Cronecker's delta, α is the coefficient of thermal expansion and ΔT is the temperature change. This relation for our purposes can be rewritten as follows:

$$\sigma^l = D^{lk}(\varepsilon^k - \varepsilon_T^k); \quad l,k = 1,\ldots,M, \tag{3}$$

where ε^k are the total strains and ε_T^k are strains due to temperature change only. M stands for the number of stress (strain) components, which is equal to 6 in the general case. In three dimensional case the normal expansions

$$\varepsilon_T^1 = \varepsilon_T^2 = \varepsilon_T^3 = \alpha\Delta T, \tag{4}$$

are only nonzero terms of the thermal strain state. D^{lk} is the symmetric matrix of material constants which form follows from (2).

The strain–displacement relations (components of Green's tensor) considering large displacements have the form (see Wempner, 1981):

$$\varepsilon_{ij} = \tfrac{1}{2}(u_{i,j} + u_{j,i} + u_{k,i}u_{k,j}); \quad i,j,k = 1,\ldots,3. \tag{5}$$

At an arbitrary point of a finite element for the three dimensional case it can be written as:

$$\varepsilon^k = (B_i^k + W_{ij}^k d_j)d_i; \quad k = 1,\ldots,M \quad i,j = 1,\ldots,N^e, \tag{6}$$

where N^e is the number of degrees of freedom in the finite element.

Both terms B_i^k and W_{ij}^k do not depend on nodal displacements. Their forms depend on shape functions and differential operators which appear in (5). Components of both quantities were defined in the paper of Hadid and Marcinowski (1989).

It is worth mentioning that the term W_{ij}^k is symmetric with respect to the pair i, j of subscripts.

Having at disposal the relation (6) one can obtain the strain variation $\delta\varepsilon^k$ which appears in (1):

$$\delta\varepsilon^k = (B_i^k + 2W_{ij}^k d_j)\delta d_i. \tag{7}$$

Through substitution of (3) and (7) into eqn (1) one obtains:

$$\sum_{(e)}\{[K_{im} + (G_{imn} + C_{inm} + H_{ijmn}d_j)d_n]d_m - F_i^T - N_{ij}^T d_j - \lambda F_i^P\}\delta d_i = 0, \tag{8}$$

where

$$K_{im} = \int_{V_e} B_i^k D^{kl} B_m^l \, dV, \quad G_{imn} = \int_{V_e} B_i^k D^{kl} W_{mn}^l \, dV, \quad C_{inm} = 2\int_{V_e} W_{in}^k D^{kl} B_m^l \, dV,$$

$$H_{ijmn} = 2\int_{V_e} W_{ij}^k D^{kl} W_{mn}^l \, dV, \quad F_i^T = \int_{V_e} B_i^k D^{kl} \varepsilon_T^l \, dV, \quad N_{ij}^T = 2\int_{V_e} W_{ij}^k D^{kl} \varepsilon_T^l \, dV,$$

$$i, j, m, n = 1, \ldots, N^e \quad k, l = 1, \ldots, M. \tag{9}$$

It is seen that the integration over the whole area was replaced by the integration over the initial volume of the finite elements and the appropriate summation over all elements (see Zienkiewicz, 1971). The symbol $\Sigma_{(e)}$ stands for this operation.

Here, the uniform distribution of the temperature field will be considered. The presented approach allows to consider the following loading process. First the temperature is elevated or dropped to the desired level. Accompanying deformations are determined through the nonlinear analysis procedure described elsewhere (see Marcinowski, 1994). Then the external load is applied. The deformation process for the given temperature change and for the mechanical loading defined by given value of λ is considered. It means that the equilibrium path in the load–displacement space for the given temperature change can be calculated. It is just a section of the equilibrium surface (see Fig. 2) at the given temperature change.

It is noteworthy that all terms defined in (9) are independent of current displacements. This feature was exploited in the code. These terms are calculated only once and stored on hard disk. Then during the calculation process they were retrieved and used in current calculations.

The relation (8) must be true for any virtual displacements. Thus one can conclude that the following relationship must be satisfied:

$$\{\Psi(d, \lambda)\} = \sum_{(e)}\{[K_{im} + (G_{imn} + C_{inm} + H_{ijmn}d_j)d_n]d_m - F_i^T - N_{ij}^T d_j - \lambda F_i^P\} = \{0\}. \tag{10}$$

Its solution for given value of a control parameter gives the point on the nonlinear equilibrium path. In this work any displacement parameter will be taken as the control parameter.

To obtain the solution of the set (10), the Newton-Raphson algorithm was used with the strategy proposed by Batoz *et al.* (1979). The same approach was adopted by Hadid and Marcinowski (1989).

3. SOLUTION OF GOVERNING EQUATIONS

Let us assume that the approximate solution $\{d\}^e$, λ^e at a given point on the path is known. The improved solution will be searched in the form:

$$\{d\} = \{d\}^e + \Delta\{d\}, \quad \lambda = \lambda^e + \Delta\lambda. \tag{11}$$

The linear set of algebraic equations on unknown increments $\Delta\{d\}$, $\Delta\lambda$ will be obtained from the requirement:

$$\{\Psi(\{d\},\lambda)\} = \{\Psi(\{d\}^e,\lambda^e)\} + \frac{\partial\Psi}{\partial\{d\}}\Delta\{d\} + \frac{\partial\Psi}{\partial\lambda}\Delta\lambda \cong \{0\}, \tag{12}$$

by the differentiation of the vector $\{\Psi\}$ defined in (10). The resulting i-th equation of this set has the form:

$$\sum_{(e)}(\Omega^e_{im}\Delta d_m - \Delta\lambda F^p_i) = -\Psi^e_i, \tag{13}$$

where

$$\Omega^e_{im} = K_{im} + [2G_{imn} + C_{inm} + C_{imn} + (2H_{ijmn} + H_{imjn})d^e_j]d^e_n - N^T_{im}. \tag{14}$$

Here, the superscript e means that the given value was calculated at point $\{d\}^e$, λ^e.

The set (13) is being solved iteratively and the new improved solution is calculated from (11). When the ratio

$$\frac{|\Delta\{d\},\Delta\lambda|}{|\{d\}^e,\lambda^e|} \tag{15}$$

is smaller than the assumed accuracy (usually $1*10^{-4}$), the iterative process is terminated. Here the norms are taken in the form of lengths of appropriate vectors in the $N+1$ dimensional space.

To discuss the solution strategy of the set (13) on unknown increments of Newton's iterations, let us rewrite this set in the matrix form:

$$[K_T]\Delta\{d\}_i - \Delta\lambda\{F\} = -\{\Psi\}_{i-1}, \tag{16}$$

where i stands for the iteration number at given step. It is worthy to emphasise that $[K_T]$ depends on current displacements and the temperature change (see (14) and (9)) and vector $\{F\}$ depends on external forces. The temperature factor is embedded also in $\{\Psi\}$ (see (10) and (9)). When any displacement is taken as the control parameter it is convenient to adopt the approach of Batoz and Dhatt (1979) utilised then by Hadid and Marcinowski (1989).

For the set of linear equations like (16) it is allowable to decompose the vector $\Delta\{d\}$ as follows:

$$\Delta\{d\}_i = \Delta\{\bar{d}\}_i + \Delta\lambda\Delta\{\bar{\bar{d}}\}_i. \tag{17}$$

Here, i still denotes the iteration number. Now, the set (13) is being reduced to the following sets

$$\begin{aligned}[K_T]\Delta\{\bar{d}\}_i &= -\{\Psi\}_{i-1},\\ [K_T]\Delta\{\bar{\bar{d}}\}_i &= \{F\},\end{aligned} \tag{18}$$

or, strictly speaking, to the one set with two right hand sides. We have at our disposal the constraint condition

$$\Delta\{d_m\}_i = 0, \tag{19}$$

where d_m is the displacement chosen as the control parameter. From this condition and from (17)

$$\Delta\lambda = -\Delta\{\bar{d}_m\}_i / \Delta\{\bar{\bar{d}}_m\}_i. \tag{20}$$

This approach guarantees the conservation of the symmetry and bandedness of the system (16) matrix.

4. CALCULATION OF THE NONLINEAR EQUILIBRIUM PATH

The nonlinear equilibrium path is composed of many equilibrium points in the load–displacement (or temperature change–displacement) space. Let us assume that all points on equilibrium path from its origin to the point k (including) are known (see Fig. 3). The next point on equilibrium path is to be found. The estimate solution for this very point is required. The problem is how to find this estimate solution for the assumed in advance step of the control parameter. This solution will constitute the start to Newton's iterations at this very step. The approach introduced by Hadid and Marcinowski (1989) will be utilised here with appropriate modifications. According to this approach the derivatives of vector $\{d\}$ and parameter λ at point k (Fig. 3) with respect to the control parameter are required. To obtain the succeeding derivatives one proceeds as follows.

Differentiating both sides of (10) with respect to the displacement control parameter d_m (the dot denotes this differentiation), the following relation is obtained

$$\dot{\Psi}_i(d, \lambda) = \sum_{(e)} [\Omega^e_{in} \dot{d}_n - \dot{\lambda} F^P_i] = 0, \tag{21}$$

or, in the matrix form,

$$[K_T]\{\dot{d}\} - \dot{\lambda}\{F\} = \{0\}. \tag{22}$$

This is the set of equations on unknown $\{\dot{d}\}$, $\dot{\lambda}$ ($\{d\}$, λ are known at this stage). This

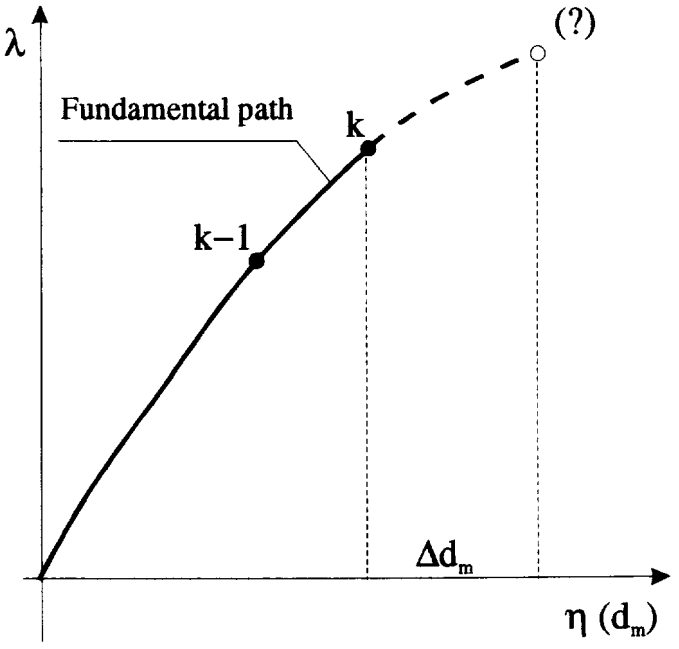

Fig. 3. Tracing strategy of a nonlinear equilibrium path.

set of equations is solved in a manner similar to the solution of the set (16), and, namely, the vector $\{d\}$ is resolved like this

$$\{\dot{d}\} = \{\dot{\bar{d}}\} + \dot{\lambda}\{\dot{\bar{\bar{d}}}\}, \tag{23}$$

and the set (21) reduced to two sets:

$$[K_T]\{\dot{\bar{d}}\} = \{0\}, \quad [K_T]\{\dot{\bar{\bar{d}}}\} = \{F\}. \tag{24}$$

The solution of the first set is trivial and the second has already been solved (see (18)). From the constraint condition $\dot{d}_m = 1$, and from (23)

$$\dot{\lambda} = 1/\{\dot{\bar{\bar{d}}}_m\}, \quad \{\dot{d}\} = \dot{\lambda}\{\dot{\bar{\bar{d}}}\}, \tag{25}$$

This means that the first derivatives are obtained without any additional efforts.

To obtain the second derivatives, let us differentiate (21) once more. The result is:

$$\ddot{\Psi}_i(d, \lambda) = \sum_{(e)}\{[\Omega^e_{im}\ddot{d}_m - \ddot{\lambda}F^P_i] + [2G_{imn} + C_{imn} + C_{inm} + (4H_{imjn} + 2H_{ijmn})d_j\dot{d}_n\dot{d}_m]\} = 0, \tag{26}$$

or, in matrix notation,

$$[K_T]\{\ddot{d}\} - \ddot{\lambda}\{F\} = \{\Theta_b\}, \tag{27}$$

where $\{\Theta_b\}$ follows from (26) and is known. To solve this set, let us resolve $\{\ddot{d}\}$ in the manner proposed earlier, i.e.,

$$\{\ddot{d}\} = \{\ddot{\bar{d}}\} + \ddot{\lambda}\{\ddot{\bar{\bar{d}}}\}. \tag{28}$$

From (27), two sets are now obtained:

$$[\dot{K}_T]\{\ddot{\bar{d}}\} = \{\Theta_b\}, \quad [K_T]\{\ddot{\bar{\bar{d}}}\} = \{F\}. \tag{29}$$

It is enough to generate the vector $\{\Theta_b\}$ and to solve the first set of these two. It is seen that the matrix of this set is still the same. It means that it was enough to triangularize K_T once and this feature was exploited in the code. This rule is true for any other higher derivatives. So, after solution of the first set and from the constraint condition $\ddot{d}_m = 0$ one obtains:

$$\ddot{\lambda} = -\{\ddot{\bar{d}}_m\}/\{\ddot{\bar{\bar{d}}}_m\}, \tag{30}$$

and the full expression on $\{\ddot{d}\}$ from (28).

Higher derivatives are obtained after differentiating the set (26) second, third etc. time. For the third derivative the resulting set is:

$$\dddot{\Psi}_i(d, \lambda) = \sum_{(e)}\{[\Omega^e_{im}\dddot{d}_m - \dddot{\lambda}F^P_i] + [6G_{imn} + 3(C_{imn} + C_{inm})]\ddot{d}_n\dot{d}_m$$
$$+ 6H_{ijmn}d_j\dot{d}_n\ddot{d}_m + 6(H_{ijmn} + H_{imjn})\dot{d}_jd_n\ddot{d}_m + 6H_{ijmn}\dot{d}_j\dot{d}_n\dot{d}_m\} = 0. \tag{31}$$

The solution method and the constraint condition are the same as in the case of the second derivative. One should generate the vector as the counterpart of $\{\Theta_b\}$. For higher derivatives they are more and more complicated, and their generation is very time consuming.

As the result of this procedure $\{\dot{d}\}$, $\{\ddot{d}\}\{\dddot{d}\}$, $\dot{\lambda}$, $\ddot{\lambda}$, $\dddot{\lambda}$, etc., are obtained. On the basis of these quantities, the estimated solution for the given in advance control parameter increment $\Delta\eta = \Delta d_m$ (see Fig. 3) is constructed as the truncated Fourier expansion from the point k:

$$\{d\}^e = \{d\}^o + \{\dot{d}\}^o\Delta\eta + \frac{1}{2}\{\ddot{d}\}^o\Delta\eta^2 + \frac{1}{3!}\{\dddot{d}\}^o\Delta\eta^3 + \cdots \tag{32}$$

$$\lambda^e = \lambda^o + \dot{\lambda}^o\Delta\eta + \frac{1}{2}\ddot{\lambda}^o\Delta\eta^2 + \frac{1}{3!}\dddot{\lambda}^o\Delta\eta^3 + \cdots, \tag{33}$$

where the superscript ^{o} means that the given value was calculated at the last (0–old) point on the path and it is the point k in Fig. 3.

In the applications presented below, the Fourier expansions were confined to four terms shown in (32) and (33) because the numerical effort required to obtain the higher derivatives is too big in comparison with expected benefit in the general performance of path tracing procedure.

Taking the estimated solution in such a form enables us to adopt comparatively large increments of the control parameter (see Hadid and Marcinowski, 1989).

In zones where the tangent to the path is nearly vertical the procedure fails, one has to change the control parameter. New displacements should be chosen. There always exists the displacement which enables the continuation of the tracing process. In the code exploited in the presented examples, the change of the displacement control parameter was conducted automatically when the convergence suddenly dropped. As a new control parameter was selected, the one for which the relative increment in the last step was the biggest (see Marcinowski and Antoniak, 1994). This procedure guarantees that the paths like these presented below can be calculated in a single run of the program.

5. APPLICATION TO THIN AND THICK SHELL STRUCTURES

The above presented algorithm can be adopted without any significant changes to shell structures provided the degenerated, isoparametric finite element is used. The element originally introduced by Ahmad *et al.* (1970) and then completed by Pawsey and Clough (1971) and Zienkiewicz *et al.* (1971) was properly extended on geometrically nonlinear range by Hadid and Marcinowski (1989). Here, the parabolic version of this very element with eight nodes and five degrees of freedom at every node ($N^e = 40$) with the tracing strategy described above was used. The vector of nodal displacements is composed of three displacements (u, v, w in global coordinates) and two independent rotations φ_x and φ_y defined properly at any point of the middle surface of a shell (see Hadid and Marcinowski, 1989).

It is worth mentioning that the shell theory is introduced on the level of finite element discretization and it is the feature of the degenerated element applied here. The adopted displacement approximation (see Ahmad *et al.*, 1970) is adequate to the five parameter shell theory (Mindlin-Reissner's theory) appropriate for thin and thick shells.

The strain vector which appears in (3) has five components ($M = 5$), namely,

$$\{\varepsilon\} = \{\varepsilon_{x'}, \varepsilon_{y'}, \varepsilon_{x'y'}, \varepsilon_{x'z'}, \varepsilon_{y'z'}\}, \tag{34}$$

where x', y', z' are the axes of the local coordinate system at any point of the element and the axis z' is perpendicular to the middle surface of the shell. In a case of uniformly distributed temperature change the vector $\{\varepsilon_T\}$ which appears in (3) has the form:

$$\{\varepsilon_T\} = \Delta T\alpha\{1, 1, 0, 0, 0\}, \tag{35}$$

where ΔT stands for the uniform temperature change and α is the coefficient of thermal expansion.

All expressions (9) which then appear in succeeding steps of the procedure were determined with the help of the Gauss integration scheme by reduced integration technique suggested by Pawsey and Clough (1971) and Zienkiewicz *et al.* (1971). Two Gauss points were used in every of the three integration directions.

6. ILLUSTRATIVE EXAMPLES

As the first example, the problem presented by Tsai and Palazotto (1991) was solved here to verify the correctness of the present approach in a purely mechanical problem. The shell is loaded by the concentrated force applied at its centre. The geometry and material properties for the problem are shown in Fig. 4. In this figure the fundamental equilibrium paths obtained for three meshes (2×2, 2×4 and 3×6 elements on the quarter of the panel, respectively) were compared with the path obtained by Tsai and Palazotto (1991). It is seen that only path for 2×2 mesh differs significantly from the one of Tsai and Palazotto (1991). Solutions for the meshes 2×4 and 3×6 elements are nearly exactly the same and coincide with the original quite well. It is noteworthy that as far as the initial and final stable segments are concerned the 2×2 mesh is quite sufficient.

To explain precisely the bucking phenomenon which takes place in this very case the bifurcation path was calculated here as well. For the purpose of this additional analysis the half of the panel was divided into 16 elements. On the contrary to the fundamental path the bifurcation path is very smooth and regular. In Fig. 4 it is the curve B_1, B_2, and actually it is the spatial loop which in this projection seems to be just a single curve. Details of the procedure used here to locate bifurcation points and calculate the bifurcation path were presented by Marcinowski (1994) and adopted by Marcinowski and Antoniak (1994) to the numerical solution of the very similar problem. The whole bifurcation path is unstable and additional plot the force vs any displacement which activates during bifurcation (e.g., horizontal displacement of the central node) allows to classify both bifurcation points as unstable symmetrical points of bifurcation (see Thompson and Hunt, 1994).

Knowledge of the bifurcation path allows to explain in what manner the buckling phenomenon proceeds. The fundamental path between bifurcation points B_1 and B_2 and the bifurcation path itself are unstable. All configurations along the fundamental path from

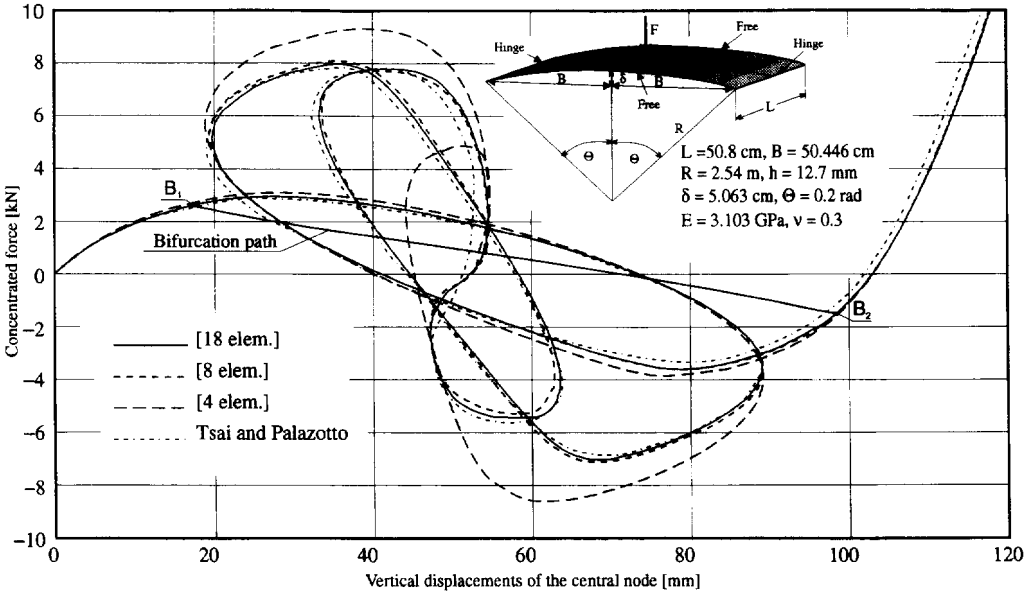

Fig. 4. Geometrically nonlinear response of the cylindrical panel.

the origin to the first bifurcation point B_1 (2604.3 N) are stable. When the force exceeds this value the panel will buckle adopting unsymmetrical configuration which is characteristic for the bifurcation mode. This configuration is unstable and the motion will be continued till the inverted symmetrical configuration is adopted. This configuration is located on the final branch of the fundamental path above B_2 (-1489.2 N) and is stable. The phenomenon itself is dynamic in its nature and as a matter of fact the problem should be treated not as a quasi static but as a dynamic one at least during the sudden transition (Riks *et al.*, 1994).

As the second example the nonlinear response of the cylindrical panel due to the concentrated force applied at its centre and temperature changes will be examined. The geometry and material parameters of the considered shell are shown in Fig. 5. It is seen that the shape slightly deviates from the symmetry with respect to the central longitudinal axis. This geometry can be treated as the cylindrical segment with geometrical imperfections.

The panel is supported along its two rectilinear edges and both arches are free. The mode of the support is hinge, i.e., all three displacements (u, v, w) and rotation with respect to the normal to the edge (φ_x) are zeros. The rotation with respect to the tangent to the edge (φ_y) is not zero (see Fig. 5).

Due to the symmetry with respect to axis $Y = L/2$ only half of the panel was discretized (see Fig. 5). Eight elements were used and such a division leads to 105 dof. First the load–displacement equilibrium path was calculated. In Figs 6 and 7 the projection of the nonlinear equilibrium path on load-vertical displacement of nodes 5 and 7 subspaces, respectively, are shown. In this case there is no temperature effect included. It is worth mentioning that there exist many unstable equilibrium configurations between the initial and final stable segments of the path. Such characteristic loops were obtained numerically earlier for panel of similar dimensions (see Marcinowski and Antoniak, 1994). Analysing the phenomenon experimentally one can observe that when the load reaches the level of the first limit point the panel snaps and adopts finally the inverted configuration which corresponds to a point on the final branch of equilibrium path. Using displacement control method in the experiment (Marcinowski and Antoniak, 1994) it is possible to locate intermediate points between initial and final branches of the equilibrium path but also in this case it is impossible to trace unstable configurations along these loops. The presence of such configurations is only manifested by sudden local snapping distinctively registered during the experiment (Marcinowski and Antoniak, 1994).

In Fig. 8, nonlinear relationships between temperature changes and vertical displacements of several nodes are shown. In calculation of this path the external load was

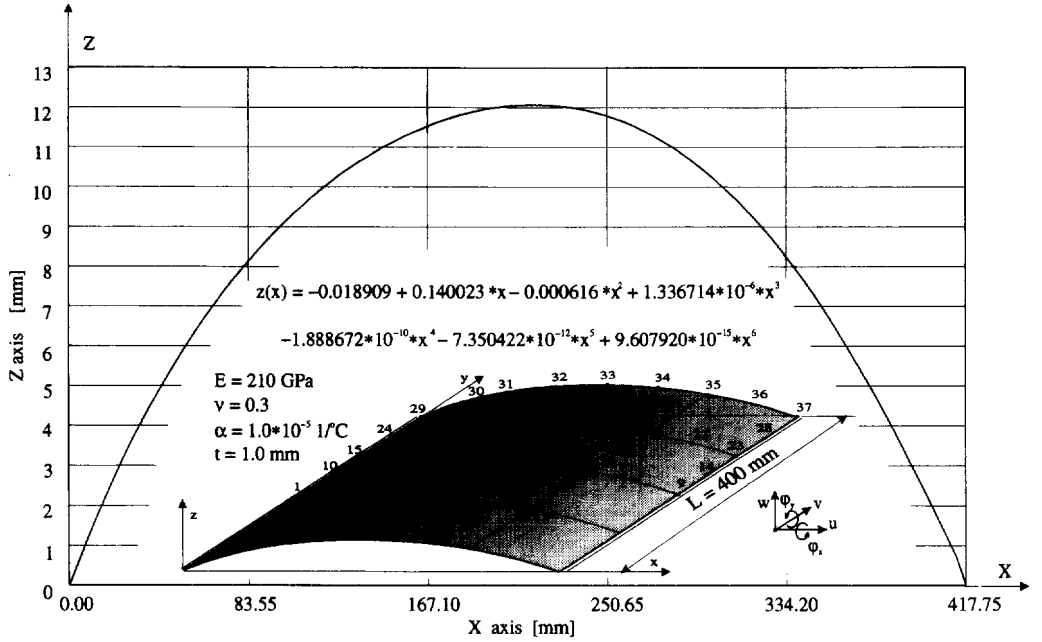

Fig. 5. Semi cylindrical steel panel.

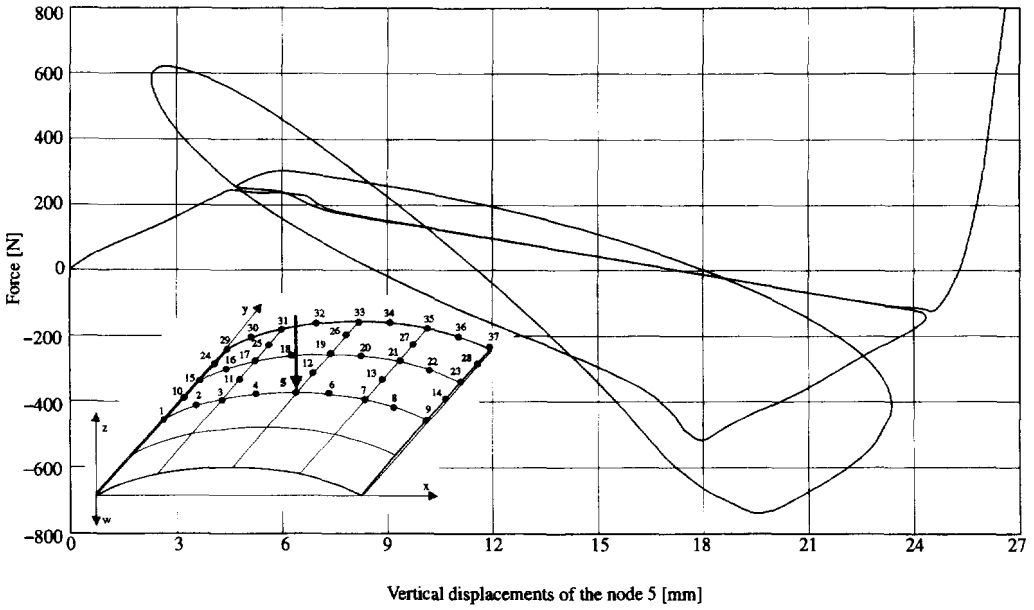

Fig. 6. Force vs nodal displacement path at reference temperature.

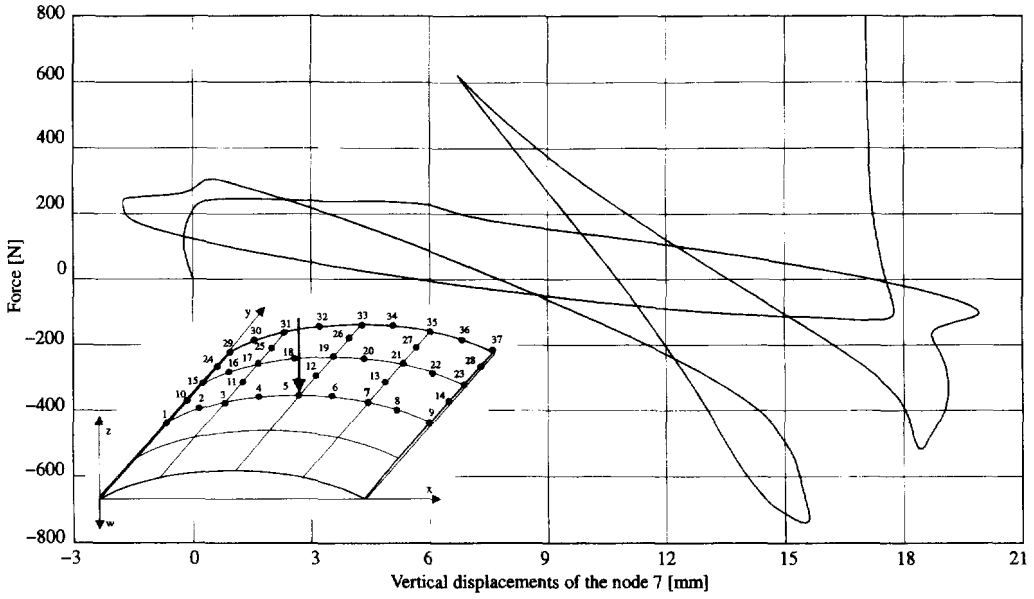

Fig. 7. Force vs nodal displacement path at reference temperature.

not included. It means that purely thermal process (process of $P+\lambda\Delta T$ type, where P was taken to be zero) was considered. This path was obtained on the basis of the procedure described by Marcinowski (1995).

Taking several configurations from those shown in Fig. 8 as a starting point to calculation of the load–displacement relationship in various temperature conditions, has enabled us to obtain equilibrium paths shown in Figs 9 and 10. Every curve represents the collection of equilibrium configurations for the given temperature change, measured with respect to the initial environmental conditions (reference temperature), and various values of the concentrated force. Those are just cross-sections of the equilibrium surface mentioned in the introduction.

In Figs 9 and 10, only initial segments of nonlinear equilibrium paths were shown. It is worth mentioning that their shape was also very complicated, sometimes similar to paths from Figs 6 and 7. Paths for $\Delta T = 0°C$ are just the ones shown in Figs 6 and 7 (their initial segments, strictly speaking).

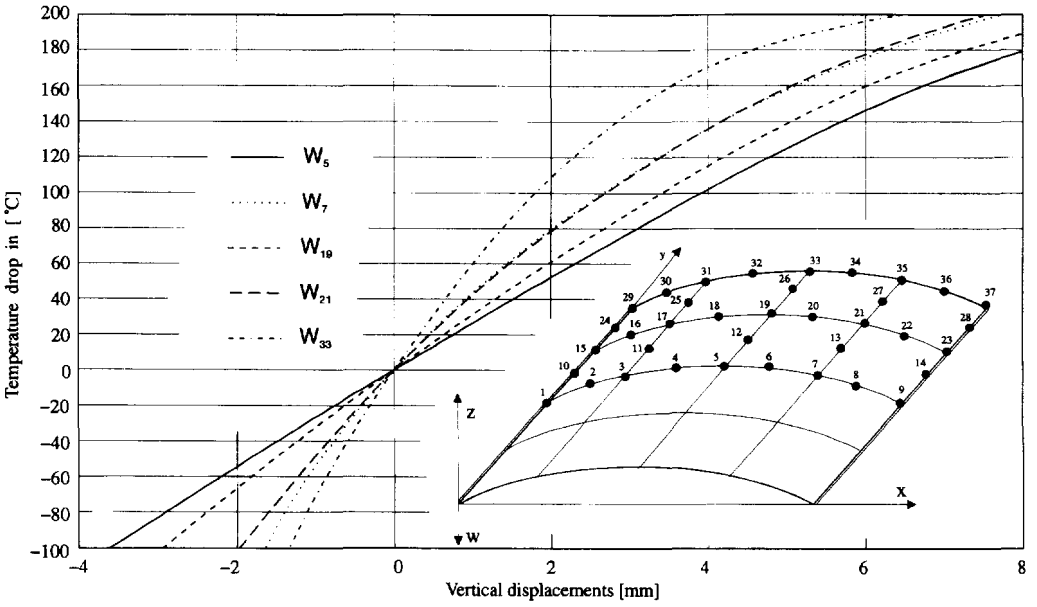

Fig. 8. Temperature change–displacement paths.

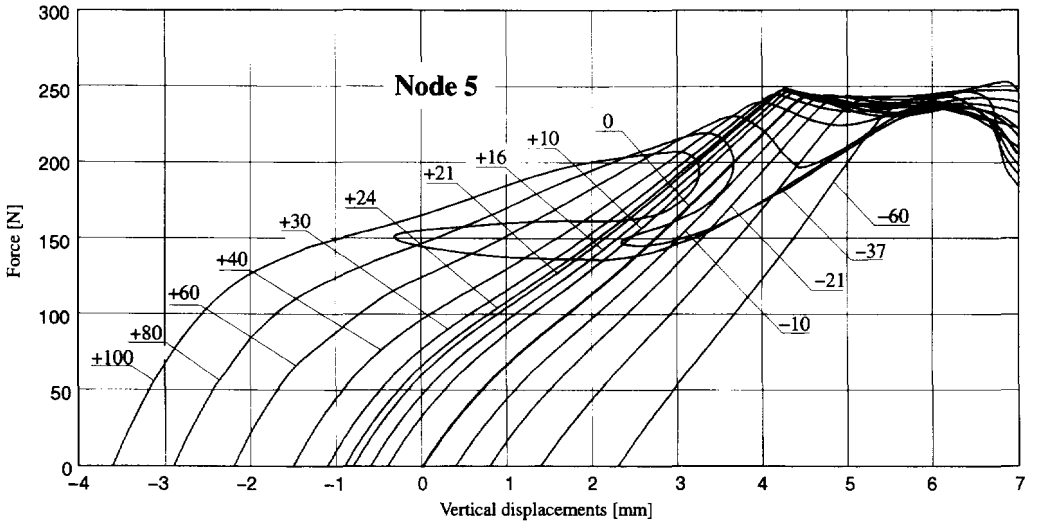

Fig. 9. Force vs nodal displacement curves.

This family of paths enabled us to construct the critical force vs temperature change relationship which was shown in Fig. 11. In fact, it is the stability boundary (see Husein, 1981) and its knowledge is the most important from the practical point of view.

It is apparent from this plot that in the vicinity of the reference temperature the elevation of the temperature cause raise of the critical force while its drop cause critical force decrease. For temperature changes smaller than $-20°C$ and higher than $+20°C$ this relationship is inverse. When temperature elevation exceeds 40°C the second limit point appears on the higher level than the primary limit point (see Figs 9 and 10). Displacements accompanying these critical points are higher of course but as a matter of fact the part of the path preceding the second limit point is stable. It is worthy to note that no bifurcation points were detected and it is probably due to the fact that the considered geometry was not symmetric, it was in fact imperfect (see Fig. 5).

From the plot and the table shown in Fig. 11 one can read the value of the critical force for various temperature changes in reference to the considered shell. From the engineering point of view this information would be very important.

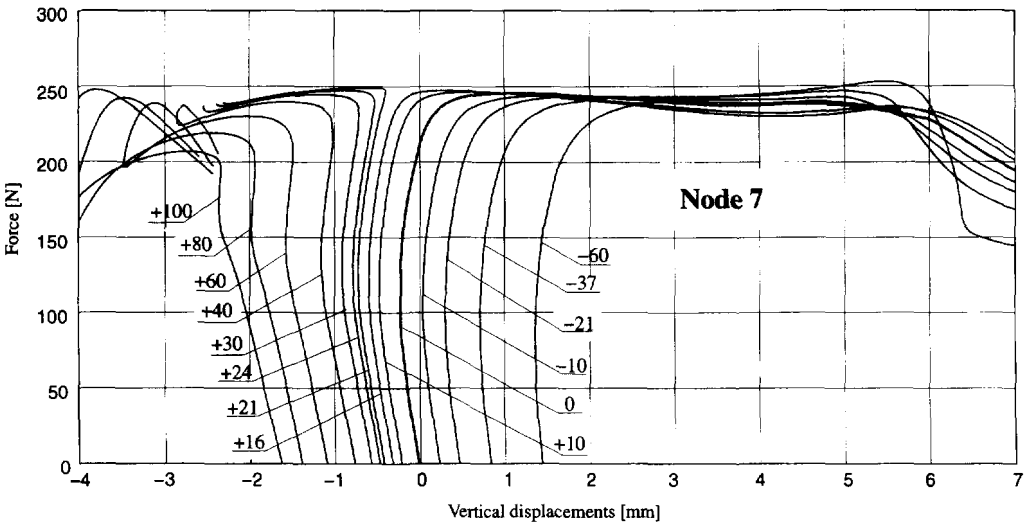

Fig. 10. Force vs nodal displacement curves.

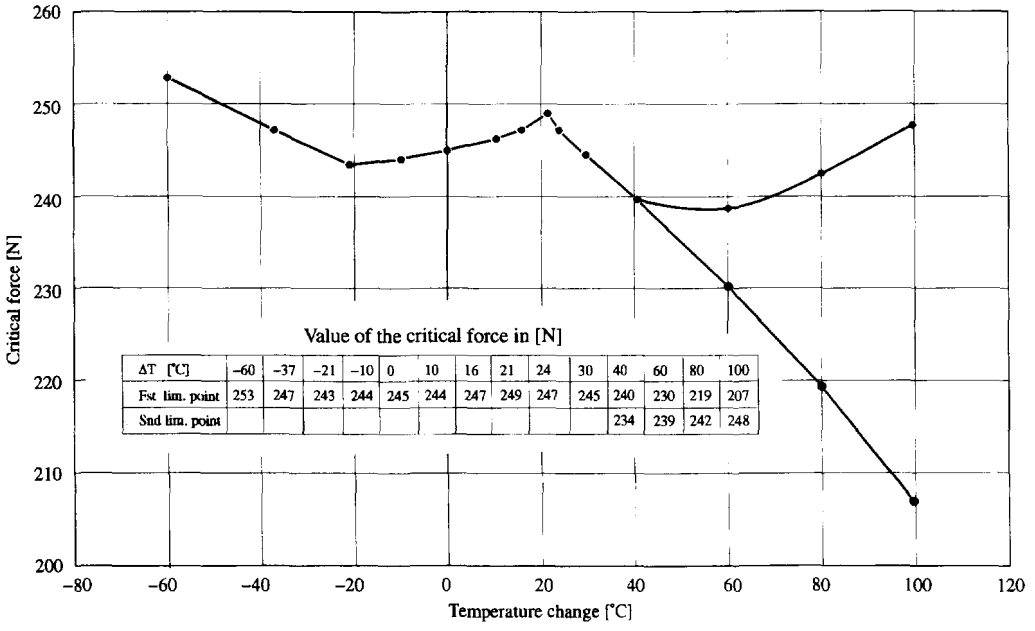

ΔT [°C]	-60	-37	-21	-10	0	10	16	21	24	30	40	60	80	100
Fst. lim. point	253	247	243	244	245	244	247	249	247	245	240	230	219	207
Snd lim. point											234	239	242	248

Fig. 11. Temperature change—critical force dependence.

7. FINAL REMARKS AND CONCLUSIONS

There is no doubt that the temperature change is a very important factor as far as the shell stability is concerned. For shells sustaining the lateral loading and undergoing the variable environmental conditions the problem is of the highest importance. The smallest change in geometry induced by the temperature change can lead to a significant stiffness change.

Only nonlinear, large displacement analysis of shell deformations due to the external load and the temperature changes seems to be the proper approach to this problem and this approach was applied in the paper.

The algorithm presented here enables to construct load–displacement equilibrium paths for a given value of the temperature change. Analysing these paths, one can estimate the critical load for given temperature change. As a result the stability boundary can be determined.

The examples inserted in the paper reveal that within the range of the adopted assumptions the formulated problem was solved properly.

As far as the numerical analysis is concerned the following conclusions can be drawn:

(i) The convergence of the problem with external loads and temperature changes treated in the manner shown above is slower than the convergence of the problems with solely external loads.
(ii) The finite element used by Hadid and Marcinowski (1989) for mechanical fields has proved to be adequate also for thermo-mechanical problems.
(iii) For purposes of the performed analysis a comparatively small number of finite elements was sufficient.

The assumptions of the isotropy and the linear elasticity of materials and independence of material properties on temperature do not confine the problem. The most interesting phenomenon, from the engineering point of view, takes place at a comparatively small ($\pm 100°C$) temperature change interval. In such conditions all material parameters can be treated as temperature independent because their values vary less than 10%. The presented algorithm is, however, general enough to include temperature dependent material parameters without significant difficulties.

The last remark refers to the tracing strategy adopted in the present paper. On the contrary to the opinion expressed by Tsai and Palazotto (1991) it was possible to trace such complicated equilibrium paths using "displacement control" method with the procedure of the automatic choice of a displacement parameter.

REFERENCES

Ahmad, S., Irons, B. M. and Zienkiewicz, O. C. (1970). Analysis of thick and thin shell structures by curved finite elements. *Int. J. Num. Meth. Engng* **2,** 419–451.

Batoz, J. L. and Dhatt, G. (1979). Incremental displacement algorithms for nonlinear problems. *Int. J. Num. Meth. Engng* **14,** 1262–1267.

Hadid, H. A. and Marcinowski, J. (1989). Nonlinear stability analysis of elastic shells. In: 10 *Years of Progress in Shell and Spatial Structures*, 30 Anniv. of IASS (ed. F. del Pozo, A. de las Casas), Cedex—Laboratorio Central de Structuras y Materiales, Madrid, 1989.

Huang, N. N. and Tauchert, T. R. (1991). Large deformations of laminated cylindrical and doubly-curved panels under thermal loading. *Comput. Struct.* **41,** 303–312.

Husein, K. (1975). *Nonlinear Theory of Elastic Stability*, Noordhoff, Leyden.

Lien-Wen Chen and Lei-Yi Chen (1990). Thermal buckling analysis of laminated cylindrical plates by the finite element method. *Comput. Struct.* **34,** 71–78.

Lien-Wen Chen and Lei-Yi Chen (1991). Thermal postbuckling behaviors of laminated composite plates with temperature-dependent properties. *Comput. Struct.* **19,** 267–283.

Marcinowski, J. (1994). Bifurcation points and branching paths in the nonlinear stability analysis of shell structures. *J. Theoret. Appl. Mech.* **32,** 637–651.

Marcinowski, J. (1995). Large deformations and instability of shell structures induced by the temperature changes. *Arch. Civil Engng*, **XLI,** 13–28.

Marcinowski, J. and Antoniak, D. (1994). Stability of the cylindrical panel. Experimental investigation and numerical analysis. *Engng Trans.* **42,** 61–74.

Meyers, C. A. and Hyer, M. W. (1991). Thermal buckling and postbuckling of symmetrically laminated composite plates. *J. Thermal Stresses* **14,** 519–540.

Pawsey, S. F. and Clough, R. W. (1971). Improved numerical integration of thick shell finite element. *Int. J. Num. Meth. Engng* **3,** 575–586.

Riks, E., Rankin, Ch. C. and Brogan, F. A. (1994). On the solution of mode jumping phenomenon in thin walled shell structures. Report LR-777, Delft University of Technology, Faculty of Aerospace Engineering, 1994.

Sivakumaran, K. S. (1990). Finite deflections of loosely clamped symmetrically laminated rectangular plates subjected to temperature fields. *J. Thermal Stresses* **13,** 297–313.

Thompson, J. M. T. and Hunt, G. W. (1973). *A General Theory of Elastic Stability*, Wiley, Chichester.

Thornton, E. A. (1993). Thermal buckling of plates and shells. *Appl. Mech. Rev.* **46,** 485–506.

Tsai, C. T. and Palazotto A. N. (1991). Nonlinear and multiple snapping responses of cylindrical panels comparing displacement control and Riks method. *Comput. Struct.* **41,** 605–610.

Wempner, G. (1981). *Mechanics of Solids with Applications to Thin Bodies*, Sijthoff & Noordhoff, Alphen aan den Rijn.

Zienkiewicz, O. C. (1972). *Finite Element Method*, Arkady, Warszawa (in Polish).

Zienkiewicz, O. C., Taylor, R. L. and Too, J. M. (1971). Reduced integration technique in general analysis of plates and shells. *Int. J. Num. Meth. Engng* **3,** 275–290.